Steady-state ionization-balance calculations for a selenium plasma

J. Abdallah, Jr., R. E. H. Clark, and J. M. Peek*
Los Alamos National Laboratory, Los Alamos, New Mexico 87545
(Received 8 February 1991; revised manuscript received 5 September 1991)

A steady-state model is used to calculate the ionization balance for a selenium plasma at electron temperatures where the Ne-like stage is dominant. In this model, the ion distribution and free-electron density are calculated for a specified particle density and temperature. In addition, each state of a given ion is connected to appropriate states of the same ion by excitation and deexcitation and connected to the appropriate states of adjacent ions by ionization and recombination. Excited states including autoionizing states are treated explicitly. Rate coefficients for all processes are based consistently on atomic-structure calculations. The calculations indicate that hundreds of electron configurations are necessary to obtain suitable results and that electron configurations must be included consistently across ion stages. Autoionizing states are shown to be the major influence in determining the ionization balance. The use of plane-wave Born collision strengths instead of better distorted-wave collision strengths appears to have a negligible effect on the overall ion stage distribution at moderate densities. The results may explain why F-like lasing transitions were not observed in the experiments by Matthews *et al.* [Phys. Rev. Lett. **54**, 110 (1985)].

PACS number(s): 32.80.Dz, 34.80.Dp, 42.55.Vc, 52.25.Dg

Recently, experiments designed to produce soft-x-ray emission from the $3p \rightarrow 3s$ transitions of Ne-like selenium ions have received considerable attention [1–10]. High-intensity optical lasers are usually focused on target materials to produce a hot plasma of the required ionized species. Although the experiments have been successful, with significant amplifications being observed for some transitions, there still remain discrepancies between measured and predicted gain coefficients [6]. The ionization balance is the distribution of ions among the various charge states at a given density and temperature. This information is fundamental to performing any accurate spectral analysis of a plasma. Ionization-balance calculations have been presented for various elements using the low-density coronal equilibrium model [11–13]. The authors are not aware of any detailed theoretical studies of selenium ionization balance at relevant plasma conditions in the literature, and most references to ionization-balance calculations refer to unpublished sources, thus making direct comparisons difficult. The purpose of this paper is to systematically study the ionization balance of a selenium plasma, as a function of density and temperature, using a detailed configuration atomic model that includes more configurations in more ion stages than previously published kinetics calculations. The model includes detailed configuration accounting for the Mg-like, Na-like, Ne-like, F-like, and O-like ion stages of selenium. Singly excited electron configurations up to (nl), and doubly excited electron configurations up to $(nl,n'l')$, are included for each ion stage, where n and $n' \leq 5$, and l and $l' \leq 3$. Some calculations are presented for configurations up to $n=10$ and $n'=3$ to study the sensitivity of the calculations to different models. Different sets of collisional-excitation cross sections are also used to test the sensitivity of the calculations. All the atomic-structure data are evaluated using the methods of Cowan [14].

The equations describing the time (t) evolution of states in a plasma are given by

$$\frac{dN_{ip}}{dt} = F_{ip} \ . \tag{1}$$

N_{ip} is the population or number density (cm^{-3}) of ions in a particular state p of ionicity i. The ionicity is related to the charge Q by

$$i = Q + 1 \ . \tag{2}$$

There is a rate equation (1) for every state ip included in the plasma model. The function F_{ip} consists of a sum of terms that describes the net production rate for the state ip. Each term describes a process that directly enhances or depletes the population of the state ip. Each term consists of a product of factors. These factors may include the free-electron density N_e, the population of the appropriate initial state N_{jq}, and the rate coefficient for the process in question. For electron-collision processes, the rate coefficient is dependent on the electron temperature. For spontaneous processes, no factors of N_e appear, and rate coefficients are independent of electron temperature. Explicit knowledge of the initial and final states for each process included is required. The plasma is considered to be optically thin, thus all photons produced by radiation-generating processes escape from the system. Furthermore, no hydrodynamic effects or continuum lowering effects are included. Reference [15] contains a compilation of the formulas and methods specifically used.

For the present purposes, only the steady-state solution of Eq. (1) is sought. For a given total particle density N and electron temperature T, as time becomes infinite, the population of each ion species ip approaches a constant value, and Eq. (1) becomes

$$F_{ip} = 0 \ . \tag{3}$$

Equation (3) forms a set of coupled algebraic equations involving all the unknown populations N_{jq} and N_e. The equations are linear in the populations N_{jq}. The conditions of charge neutrality

$$N_e = \sum_{j,q} (j-1) N_{jq} \ , \tag{4}$$

and particle conservation

$$N = \sum_{j,q} N_{jq} \ , \tag{5}$$

are also imposed. It is possible to simultaneously satisfy Eqs. (3)–(5) by standard techniques. Equations (3) and (4) are solved by standard linear algebraic methods for a specific value of N_e and T. N_e is then varied in Eqs. (3) and (4) until a solution N_{jq} is found, which satisfies Eq. (5) for a given N. Note that the state populations and ion balance are calculated for a total number density N and the electron temperature T. T determines the Maxwell electron-velocity distribution used to evaluate rate coefficients appearing in the F's, and N is used for the condition expressed in Eq. (5). The solution ensures that all ion states simultaneously exist in a steady state.

The solution of Eqs. (3)–(5) approaches the coronal limit at low densities and approaches local thermodynamic equilibrium (LTE) at high densities. If the electron density is sufficiently low to make collisional-excitation rates small compared to radiative decay rates, then the excited-state populations are negligible. The coronal model is a steady-state solution involving only the ground states of the ions through net ionization and recombination processes. In LTE, the rates of forward processes are exactly balanced by the rates of their reverse processes; hence no detailed cross sections are required, and the population distribution is determined solely by state energies and statistical weights. The current steady-state model is much more computationally intensive than either the coronal or LTE models, which can be given in terms of simple expressions [11,14].

The rate coefficients appearing implicitly were evaluated using the methods that have been used successfully for computing electron-impact cross sections for neutral barium [16], for computing the transmission of x rays through an aluminum plasma [17], and for computing an assortment of atomic physics data for all the ion stages of titanium [18]. The use of the codes is discussed in greater detail in Refs. [19–23]. The methods used are described in great detail in Cowan's book and will not be discussed further. The atomic-structure calculations were performed for Se^{22+}, Se^{23+}, Se^{24+}, Se^{25+}, and Se^{26+}. Table I describes the sets of configurations that were used for each ion stage. It also summarizes the number of processes calculated. The amount of data calculated is too large to be presented in detail here. The sets of configurations were varied to study the effects of different states on the ion distribution. For example, Table II describes a more limited set of configurations than Table I, which is used for various model calculations.

Configuration-based values for energies and cross sections were used so that the ion-balance calculations could be carried out without restricting the number of configurations included in the basis set. Calculations with fine-structure levels, intermediate coupling, and configuration interaction are required for predicting realistic spectra and calculating gain coefficients. Detailed fine-structure calculations for more limited sets of

TABLE I. Summary of data calculated for each ion stage of selenium, NC is the number of configurations, NIT is the number of internal transitions, NPI is the number of photo or collisional ionizations, and NAI is the number of autoionizations. Here n, n', and n'' correspond to principle quantum numbers; and l, l', and l'' correspond to orbital angular quantum numbers.

Ion	NC	NIT	NPI	NAI	Configurations
Se^{22+}	144	1304	391	274	$1s^2 2s^2 2p^6 3lnl$
					$1s^2 2s^2 2p^5 3l3l'n''l''$
					$1s^2 2s^1 2p^6 3l3l'n''l''$
Se^{23+}	143	1573	539	302	$1s^2 2s^2 2p^6 nl$
					$1s^2 2s^2 2p^5 nln'l'$
					$1s^2 2s^1 2p^6 nln'l'$
Se^{24+}	221	2574	761	510	$1s^2 2s^2 2p^6$
					$1s^2 2s^2 2p^5 nl$
					$1s^2 2s^1 2p^6 nl$
					$1s^2 2s^2 2p^4 nln'l'$
					$1s^2 2s^1 2p^5 nln'l'$
					$1s^2 2p^6 nln'l'$
Se^{25+}	233	2784	785	572	$1s^2 2s^2 2p^5$
					$1s^2 2s^1 2p^6$
					$1s^2 2s^2 2p^4 nl$
					$1s^2 2s^1 2p^5 nl$
					$1s^2 2p^6 nl$
					$1s^2 2s^2 2p^3 nln'l'$
					$1s^2 2s^1 2p^4 nln'l'$
					$1s^2 2p^5 nln'l'$
Se^{26+}	234	2796			$1s^2 2s^2 2p^4$
					$1s^2 2s^1 2p^5$
					$1s^2 2p^6$
					$1s^2 2s^2 2p^3 nl$
					$1s^2 2s^1 2p^4 nl$
					$1s^2 2p^5 nl$
					$1s^2 2s^2 2p^2 nln'l'$
					$1s^2 2s^1 2p^3 nln'l'$
					$1s^2 2p^4 nln'l'$
					$n,n',n'' \leq 5$
					$l,l',l'' \leq 3$

TABLE II. Summary of data for limited model calculations.

Ion	NC	NIT	NPI	NAI	Configurations
Se^{23+}	27	151	61	18	$1s^2 s^2 2p^6 nl$
					$1s^2 2s^2 2p^5 3snl$
					$1s^2 2s^1 2p^6 3snl$
Se^{24+}	19	99	47	0	$1s^2 2s^2 2p^6$
					$1s^2 2s^2 2p^5 nl$
					$1s^2 2s^1 2p^6 nl$
Se^{25+}	20	109			$1s^2 2s^2 2p^5$
					$1s^2 2s^1 2p^6$
					$1s^2 2s^1 2p^4 nl$
					$1s^2 2s^1 2p^5 nl$
					$n \leq 5$
					$l \leq 2$

configurations are planned for the future.

Oscillator strengths were calculated for all possible dipole-allowed transitions between configurations. The oscillator strengths are used to compute the rate coefficients (Einstein A coefficients) for spontaneous radiative decay to states of lower energy.

Electron collisional-excitation cross sections were calculated for all possible transitions between configurations, including excited-to-excited transitions and excitations to autoionizing states. The plane-wave Born (PWB) model [14] modified to give better results at near-threshold electron energies was used. The distorted-wave (DW) cross sections were used for the comparison studies. The rate coefficients for excitation are obtained by numerically integrating the cross section over a Maxwellian distribution for the free electrons at the appropriate temperature. The rate coefficient for the reverse process, collisional deexcitation (superelastic collisions), is calculated using the principle of detailed balance.

Photoionization cross sections are used for generating radiative recombination rate coefficients from the principle of detailed balance. Radiative recombination is the reverse process of photoionization; an incident electron gets captured by an ion and produces a photon. Rate coefficients are obtained by numerically integrating the cross section over a Maxwellian distribution for the electrons at the appropriate temperature. Cross sections are calculated for all possible photoionizations from the set of configurations of the target ion stage to the set of configurations of the next higher ion stage.

When an ion is excited into a state that lies above the ionization limit, that state may autoionize, that is, spontaneously eject a free electron leaving the ion in a state of the next higher stage. Rate coefficients for the reverse process, dielectronic recombination, are calculated using the principle of detailed balance. Autoionization rates are calculated for all possible autoionizing transitions to states in the next higher ion stage.

Since autoionizing states are considered explicitly, the effect of density on dielectronic recombination is included dynamically. If an autoionizing stage is attained, either by electron collisions or dielectronic capture, the state may be quenched by radiative decay, autoionization, superelastic collsions, collisional excitation to higher-lying autoionizing states, or direct collisional ionization. This treatment of dielectronic recombination differs somewhat from the usual scheme where these states are not included explicitly, and effective rate coefficients are computed using the appropriate radiative decay and Auger rates [3–5]. The effect of density on the effective dielectronic recombination rate coefficient for selenium has been discussed by Hagelstein, Rosen, and Jacobs [4]. A comparison between results of the present method with those using effective rate coefficients is beyond the scope of this paper and is planned to be the subject of a future publication. However, effective rate coefficients computed with the present atomic physics data compare very favorably with previous estimates. The net total rate coefficient for dielectronic recombination from the F-like ion to the Ne-like ion was calculated using the Auger and radiative rates summarized in Table I to check for possible errors. The calculated value at an electron temperature of 1 keV is 3.30×10^{-11} cm^3 sec^{-1}, which agrees well with estimates of $(2.8-3.5)\times10^{-11}$ presented in Ref. [3]. In fact, the present calculation includes doubly excited states up to $(5l,5l')$, more than in previous calculations.

Collisional ionization occurs when an electron collides with an ion and strips off another electron, leaving the ion in a state of the next higher ion stage. These cross sections are calculated using fits [24] to scaled hydrogenic ionization theory [25] with binding energies obtained from the atomic-structure calculations. Rate coefficients are obtained by integrating the functional forms over a Maxwellian distribution for the electrons, which leaves an expression in terms of easy to evaluate exponential integrals. Rate coefficients for the reverse process, three-body recombination, are obtained using the principle of detailed balance. Collisional-ionization cross sections are calculated for all possible ionizations of the configurations in the target ion stage connecting to configurations of the next higher ion stage.

Solutions to Eqs. (3)–(5) were found by solving the 975×975 matrix problem encountered using the method described above, the configurations described in Table I, and rate coefficients evaluated using the methods discussed above. A range of temperatures was scanned to determine the region where the Ne-like ion stage dominates. Figure 1 shows the calculated steady-state ion fractions for Se^{22+}, Se^{23+}, Se^{24+}, Se^{25+}, and Se^{26+} as a function of temperature for particle densities of 10^{18}, 10^{19}, and 10^{20}. The ion fraction is defined as

$$f_i = N_i / N \ , \tag{6}$$

where N_i is the total number density of ions of ionicity i,

$$N_i = \sum_q N_{iq} \ . \tag{7}$$

The ion fractions are less accurate near the lower and upper charge boundaries due to the lack of contributions from other ion stages that are not included in the calculation. The results show that as the density is increased for a given temperature, the average charge state increases. This is due to the enhanced ionization from excited states as the electron density is increased. The range of electron temperatures for which the Ne-like ion stage dominates is large, and it is in general agreement with measured and observed estimates of the experimental conditions [6], which range from about 1000–1300 eV.

However, an XRASER ionization-balance calculation is referred to in Ref. [6] as a private communication. No details of the calculation are given, so detailed comparisons with the present results are not possible. The calculation predicts a $[Se^{25+}]/[Se^{24+}]$ ratio of 2.8 at the single point $N_e=5\times10^{20}$ and $kT=1000$ eV, which is contradictory to the current result that shows Se^{24+} to be the dominant ion stage. The difference is probably due to the use of consistent sets of configurations across ion stages in the current calculations. We have observed that this is especially important when the ion stage ground state

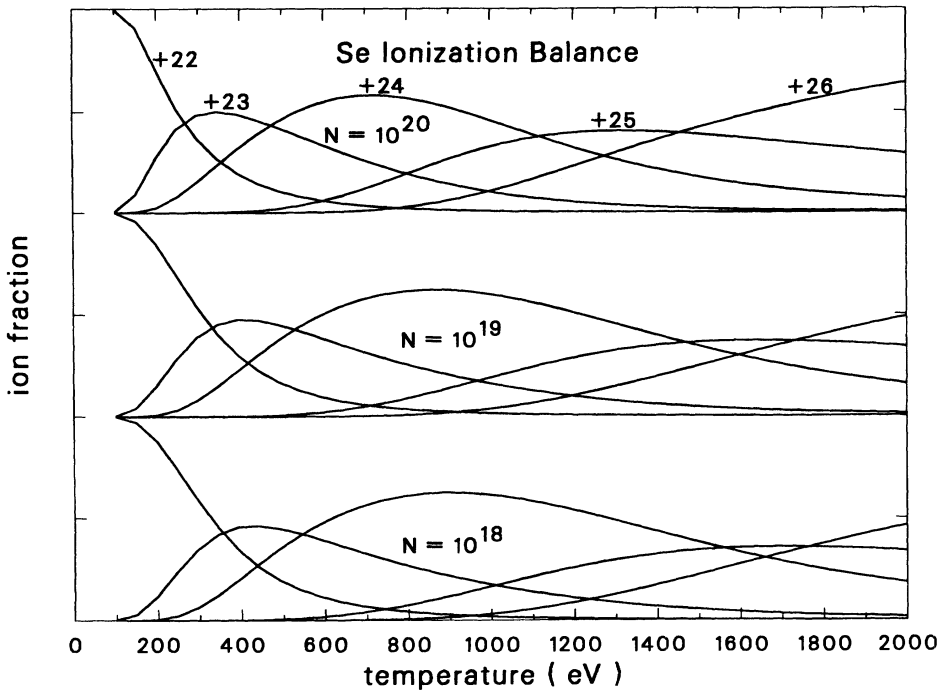

FIG. 1. Selenium ion balance as a function of temperature for particle densities of 10^{18}, 10^{19}, 10^{20}.

passes through a shell of changing principle quantum numbers (Na-like to Ne-like boundary) and when autoionizing states are included. This sensitivity has also been independently recognized by Walling *et al.* [26] and Osterheld *et al.* [27]. The present calculations may explain why lasing of the F-like lines were not observed in the experiments, because they predict that the percentage of F-like ions is small in the density and temperature range of interest, in contrast with the XRASER results.

Figure 2 shows the effect of density and temperature on the population of Ne-like selenium. The results are also compared to the coronal and LTE calculations with

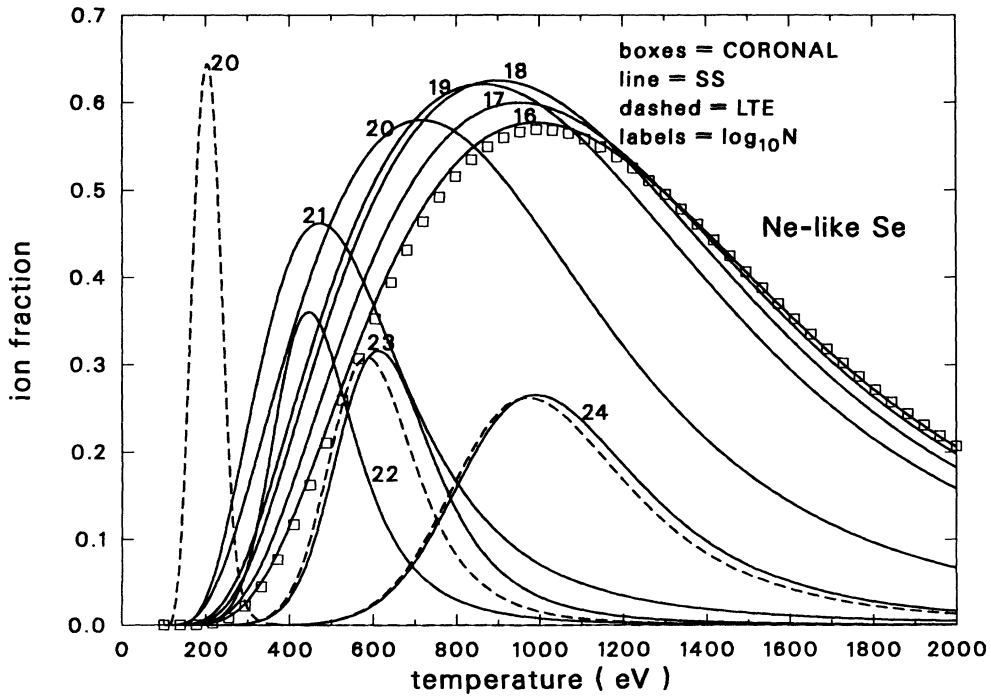

FIG. 2. The calculated ion fraction of Ne-like selenium as a function of temperature for various particle densities using the coronal, steady-state, and LTE models.

the same atomic model (Table I). The ion fraction is plotted as a function of temperature for various densities; the numerical label for each curve is $\log_{10}$ of the particle density. At low density, the steady-state and coronal results (boxes) agree. The choice of branching ratio in the coronal model is important for processes involving autoionizing states since the steady-state model treats each process explicitly. As density increases the ion-fraction curves tend to peak at lower temperatures. At about a particle density of 10^{22}, the ion fractions turn around and then begin to show LTE behavior, i.e., the curves tend to peak at higher temperatures as the density is increased. The steady-state calculations agree with LTE (dashed curves) at the highest densities. Figure 2 also shows that dielectronic recombination is treated correctly and self-consistently. The steady-state model, which uses the detailed interconnections between states, approaches the coronal calculation at low density, which uses the effective dielectronic recombination rate. At high density, the steady-state model approaches LTE, which uses only state energies and statistical weights. Thus, the steady-state calculation agrees with completely independent models that provide the correct limiting behavior at low and high density.

Autoionization and dielectronic recombination have been shown to be important for computing gain coefficients [3,4]; however, their specific effect on the ionization balance of selenium has not been demonstrated. In addition, the variation of the ionization balance with different atomic models has not been studied. Figure 3 shows the effect of autoionization (AI) and dielectronic recombination (DR) on the Ne-like ion population. The solid lines are based on the model described in Table I. The rate coefficients for autoionization and dielectronic capture in all ion stages are set to zero for the curve labeled no AI and DR, and rate coefficients just for autoionization are set to zero for the curves labeled DR only. The figure shows that autoionization and dielectronic recombination increase the peak temperature by a factor of 2 and spread the population over a large range of temperature. The triangles correspond to a small model calculation (see Table II), that uses only 19 configurations in the Ne-like stage. This calculation correlates very well with the case of no autoionization and dielectronic recombination. The figure shows that neither autoionization nor dielectronic recombination can be neglected and that their effects cause major differences in the ionization balance.

The boxes and dashed lines appearing in Fig. 3 correspond to calculations using different sets of configurations to examine their effect on the ionization balance. The boxes correspond to a calculation using a subset of the configurations described in Table I, all doubly excited electron configurations designated by $nln'l'$ were limited to $n'=3$. This calculation agrees well with the more complete solid-line model, which indicates that most of the dielectronic recombination occurs through the $nl3l'$ states. The atomic model was also expanded to study the effect of higher values of principle quantum number. The dashed line corresponds to a calculation using a modification of the set of configurations described in Table I. All singly excited electron configurations were extended to $n \leq 10$, and all doubly excited electron configurations designated by $nln'l'$ were modified to allow $n \leq 10$ and $n'=3$. The effect of higher n values is to slightly spread the ion population over temperature and

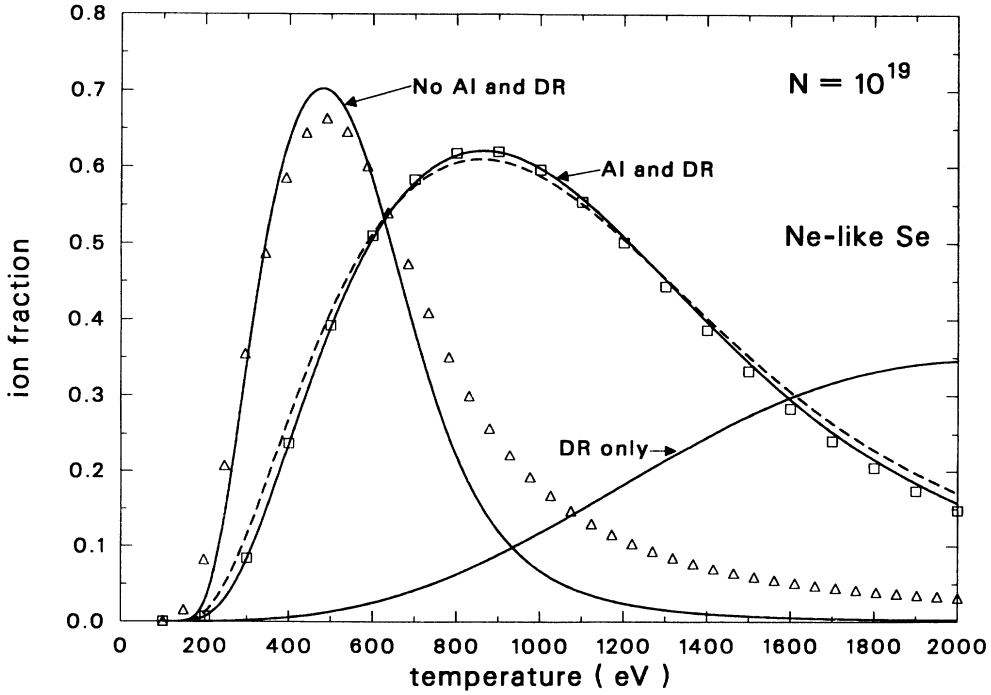

FIG. 3. The calculated ion fraction of Ne-like selenium as a function of temperatures using various configuration sets and processes (see text) at a particle density of 10^{19}.

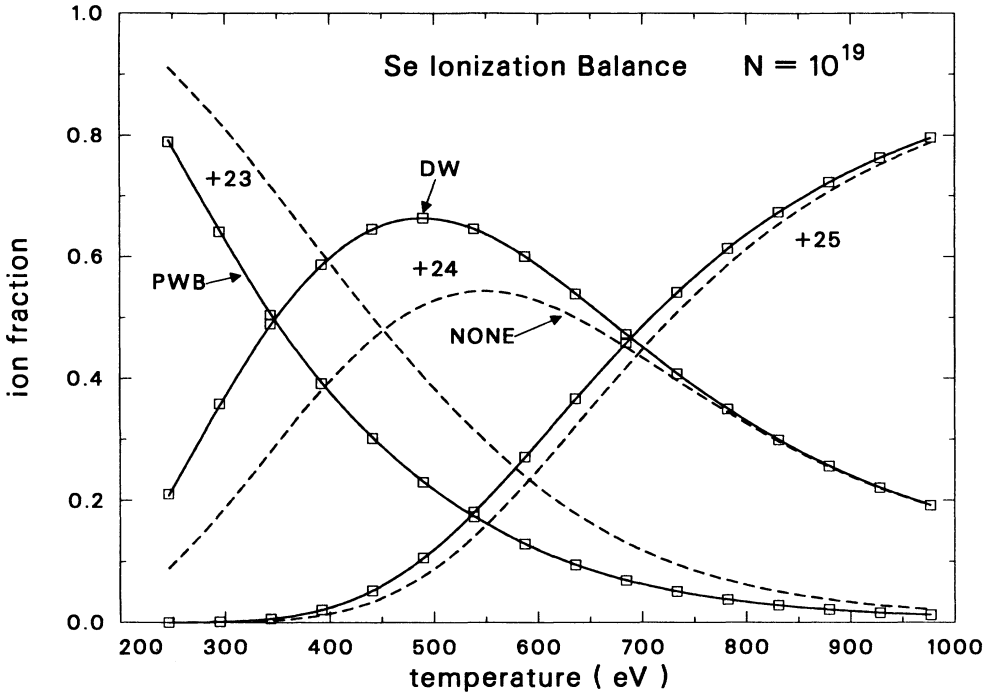

FIG. 4. The calculated ion fraction of Ne-like selenium using distorted-wave cross sections (boxes), plane-wave-Born cross section (solid), and no collisional excitation (dashed) at a particle density of 10^{19}. The shortened configuration set described by Table II was used.

to decrease its peak value slightly; however, there is no major change in the overall ion balance.

Since PWB collisional-excitation cross sections are suspect, especially near threshold, ionization-balance calculations using the distorted wave (DW) method were performed for comparison purposes. The small 19-configuration model described in Table II was used. Figure 4 compares the ionization balance calculated with both PWB and DW cross sections at a particle density of 10^{19} cm^{-3}. Note that there is no difference between the two calculations at this density. However, the dashed line, which includes no collisional transitions at all shows

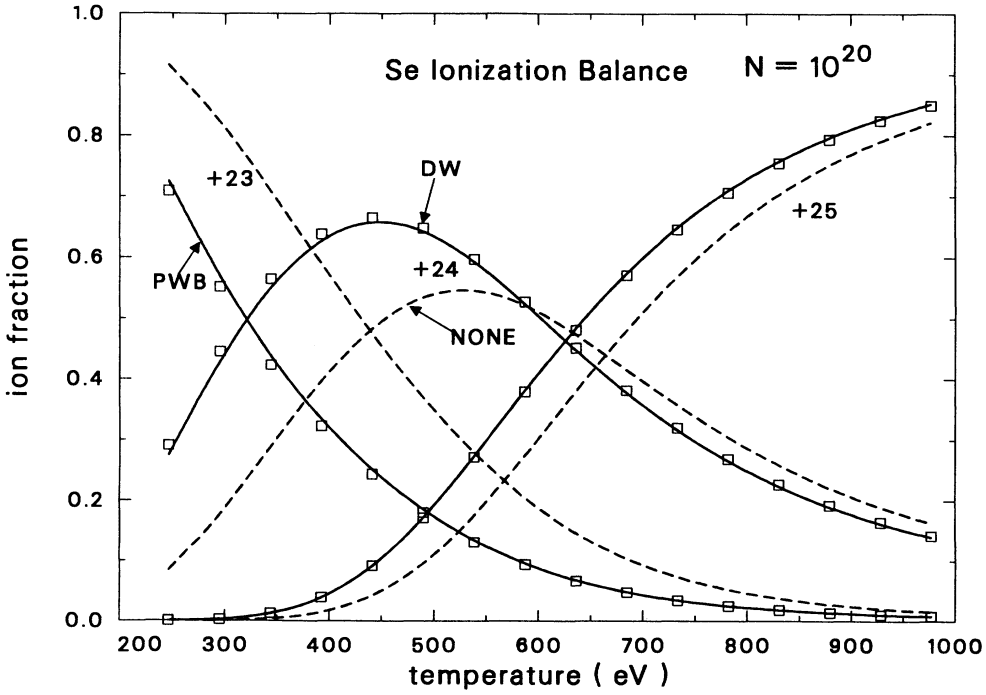

FIG. 5. Same as Fig. 4 except at a particle density of 10^{20}.

a significant difference. At this density, the role of collisional excitation is important, but it does not seem to matter if PWB or DW cross sections are used for ionization-balance calculations. As the density is increased, the populations of excited states become more significant, and the difference between the PWB and DW calculations becomes more pronounced. Figure 5 shows that at $N = 10^{20}$ slight differences in the two curves become apparent.

In conclusion, steady-state collisional-radiative ionization-balance calculations have been performed for a selenium plasma in the density and temperature domain where the Ne-like stage is important. Processes involving autoionizing states are shown to be the major factor in determining the ionization balance; hence many configurations are necessary to obtain reasonable convergence. Calculations are performed which show that PWB collision strengths are of sufficient accuracy for computing the overall ion balance at moderate densities. The calculations show that the electron temperature range where the Ne-like ion stage occurs is consistent with previous estimates of the plasma conditions from laser-induced soft-x-ray amplification experiments. However, the current results disagree by approximately an ion stage with previous estimates of the ionization balance. The differences are probably due to inconsistent choices of configurations across ion stages in the earlier calculations. The current results may explain why F-like lasing transitions were not observed experimentally.

The authors thank Raymond C. Elton for introducing us to the problem. The authors also thank C. J. Keane, D. L. Matthews, R. S. Walling, and A. L. Osterheld for informative discussions. This work was performed under the auspices of the U.S. Department of Energy.

---

*Present address: RFD 2, Green City, MO 63545.

[1] M. D. Rosen, P. L. Hagelstein, D. L. Matthews, E. M. Campbell, A. U. Hazi, B. L. Whitten, B. MacGowan, R. E. Turner, and R. W. Lee, Phys. Rev. Lett. **54**, 106 (1985).

[2] D. L. Matthews, P. L. Hagelstein, M. D. Rosen, M. J. Eckart, N. M. Ceglio, A. U. Hazi, H. Medecki, B. J. MacGowan, J. E. Trebes, B. L. Whitten, E. M. Campbell, C. W. Hatcher, A. M. Hawryluk, R. L. Kauffman, L. D. Pleasance, G. Ranbach, J. H. Scofield, G. Stone, and T. A. Weaver, Phys. Rev. Lett. **54**, 110 (1985).

[3] B. L. Whitten, A. U. Hazi, M. H. Chen, and P. L. Hagelstein, Phys. Rev. A **33**, 2171 (1986).

[4] P. L. Hagelstein, M. D. Rosen, and V. L. Jacobs, Phys. Rev. A **34**, 1931 (1986).

[5] W. H. Goldstein, B. L. Whitten, A. U. Hazi, and M. H. Chen, Phys. Rev. A **36**, 3607 (1987).

[6] B. L. Whitten, M. H. Chen, A. U. Hazi, C. J. Keane, R. A. London, B. J. MacGowan, D. L. Matthews, T. W. Phillips, M. D. Rosen, J. L. Trebes, and D. A. Whelan, in *Proceedings of the International Conference on Lasers '88,* edited by R. C. Sze and F. J. Duarte (STS, McLean, VA, 1989), and references therein.

[7] R. A. London, M. D. Rosen, M. S. Maxon, D. C. Elder, and P. L. Hagelstein, J. Phys. B **22**, 3363 (1989), and references therein.

[8] Raymond C. Elton, *X-Ray Lasers* (Academic, San Diego, 1990).

[9] J. P. Apruzese, J. Davis, M. Blaha, P. C. Kepple, and V. L. Jacobs, Phys. Rev. Lett. **55**, 1877 (1985).

[10] M. C. Coulter, J. P. Apruzese, and K. G. Whitney, Appl. Phys. B **50**, 193 (1990).

[11] C. Jordan, Mon. Not. R. Astron. Soc. **142**, 501 (1969).

[12] C. Jordan, Mon. Not. R. Astron. Soc. **148**, 17 (1970).

[13] R. Mewe, in *Proceedings of the Advanced NATO Research Workshop on Physical Processes in Hot Cosmic Plasmas, Volcano, Italy, 1989,* edited by W. Brinkmann, A. C. Fabian, and F. Giovannelli (Kluwer, Dordrecht, 1990), and references therein.

[14] R. D. Cowan, *Theory of Atomic Spectra* (University of California Press, Berkeley, CA, 1981).

[15] J. Abdallah, Jr. and R. E. H. Clark, Los Alamos Report No. LA-11926 1990 (unpublished), and references therein.

[16] R. E. H. Clark, J. Abdallah, Jr., G. Csanak, and S. P. Kramer, Phys. Rev. A **40**, 2935 (1989).

[17] J. Abdallah, Jr. and R. E. H. Clark, J. Appl. Phys. **69**, 23

[18] R. E. H. Clark and J. Abdallah, Jr., Phys. Scr. T **37**, 28 (1991).

[19] R. E. H. Clark and J. Abdallah, Jr., in *Proceedings of the International Symposium on Correlation and Polarization in Electronic and Atomic Collisions,* edited by P. A. Neill, K. H. Becker, and M. H. Kelley, National Institute for Standards and Technology Special Publication No. 789, 22 (1989).

[20] J. Abdallah, Jr., R. E. H. Clark, and R. D. Cowan, Los Alamos Manual No. LA-11436-M-I, 1988 (unpublished).

[21] R. E. H. Clark and J. Abdallah, Jr. (unpublished).

[22] R. E. H. Clark, J. Abdallah, Jr., G. Csanak, J. B. Mann, and R. D. Cowan, Los Alamos Manual LA-11436-M-II, 1988 (unpublished).

[23] J. B. Mann, At. Data Nucl. Data Tables **29**, 407 (1988).

[24] R. E. H. Clark, J. Abdallah, Jr., and J. B. Mann, Astrophys. J. **381**, 597 (1991).

[25] L. B. Golden and D. H. Sampson, J. Phys. B **13**, 2656 (1980).

[26] R. S. Walling, A. L. Oserheld, J. H. Scofield, and W. H. Goldstein (unpublished).

[27] A. L. Osterheld, R. S. Walling, W. H. Goldstein, J. H. Scofield, M. H. Chen, B. J. MacGowan, S. Maxon, and B. K. F. Young (unpublished).